Available online at www.sciencedirect.com
SCIENCE DIRECT®
Solid State Ionics 164 (2003) 97–106
SOLID STATE IONICS
www.elsevier.com/locate/ssi

Humidity sensing properties of NiO/Al_2O_3 nanocomposite materials

Salah A. Makhlouf[a,*,1], Kamal M.S. Khalil[b,2]

[a] Physics Department, Faculty of Science, United Arab Emirates University, Al-Ain 17551, United Arab Emirates
[b] Chemistry Department, Faculty of Science, United Arab Emirates University, Al-Ain 17551, United Arab Emirates

Received 30 October 2002; received in revised form 25 July 2003; accepted 25 July 2003

Abstract

Humidity sensing properties measured by impedance spectroscopy (IS) and DC conductivity for a group of high surface area nanostructured 5–30% w/w NiO/Al_2O_3 composite materials are reported. The nanocomposites were prepared via a sol–gel method, which involved mixing of the respective sol–gel precursors and the subsequent drying and calcination at 873 K for 3 h. Accordingly, nanosized NiO particles dispersed in γ-Al_2O_3 matrix were formed. Conductivity changes amount to six orders of magnitudes were observed in response to 5–90% relative humidity (RH) change in the measuring chamber. Results indicate that humidity sensing was increased with the increase of NiO content in the composite. Moreover, conductance kinetics and conduction mechanism are discussed in terms of surface texture and nanostructured morphology of the composite materials that facilitate ionic transport mechanism.

Keywords: Humidity sensing; Nanostructured; NiO/Al_2O_3; Sol–gel technique; Impedance spectroscopy

1. Introduction

Fabrication and characterization of nanostructured materials has become the subject of intense research from both theoretical point of view as well as for their potential technological applications [1–6]. In particular, the sol–gel method has received wide attention as a precursor for the synthesis of metal oxide materials of specific textural and microstructural characteristics [7,8].

Humidity sensing has become an important issue at industrial sites, medicine, food production and for human comfort [9]. Various solid state chemical sensing devices are operated on the basis of gas/solid interactions that occur at surfaces, grain boundaries, or interfaces between different materials. The unique structure of nanostructured materials, which consist of grains, grain boundaries, surfaces and pores facilitates their use as chemical sensors. Ionic type mechanism is proposed and applied to explain conductivity of such ceramics [9–11], which involves transport of protons via a Grotthuss chain reaction [12]. The high electrostatic field in the chemisorbed layer promotes dissociation of physisorbed water and produces pro-

* Corresponding author. Tel.: +971-37064765; fax: +971-37671291.
E-mail address: smakhlouf@uaeu.ac.ae (S.A. Makhlouf).
[1] Permanent address: Department of Physics, Faculty of Science, Assiut University, Assiut 71516, Egypt.
[2] Permanent address: Department of Chemistry, Faculty of Science, South Valley University, Sohag 82524, Egypt.

0167-2738/$ - see front matter © 2003 Elsevier B.V. All rights reserved.
doi:10.1016/S0167-2738(03)00307-2

tons, which are responsible for the electrical conduction, by hopping between water molecules [11]. In fact, humidity sensing by ceramics is mainly dependent on the specific surface, which in its turn depends on the available pore sizes and their distribution [13]. A variety of ceramic sensors and polymeric sensors are serving as humidity sensors based upon changes in resistance or capacitance with changes in relative humidity [9,14,15]. Ceramic thin films and electrocomposites have also been investigated for humidity sensing characteristics [16,17].

AC impedance spectroscopy (IS) is a powerful tool for investigating the electrical properties of such systems. The measurements can be performed without electrode polarization effects. Moreover, separation of bulk response from grain boundary and electrode-related phenomena is possible. The measured effective dielectric constant gives a clear idea about the nature of the bulk response showing whether it arises from the solid phase or from interfaces. Impedance data of materials that have capacitive and resistive components when represented in the Nyquist diagram [i.e. the negative of the imaginary part ($-Z''$) in the y axis and the real part (Z') in the x axis, and each point corresponding to a different frequency] lead to a succession of semicircles. In this case, the second intercept of the high frequency semicircle with the real axis is the bulk resistance of the sample. Hence, the bulk electrical conductivity is obtained. The relaxation frequency of the material is found at the apex of the Nyquist semicircle. The bulk capacitance of the material, also called the geometric capacitance [18], can be calculated and hence the bulk dielectric constant can be determined.

In the present study, the humidity sensing properties of NiO/Al_2O_3 nanocomposites are addressed. The humidity sensitivity of electrical conductivity and capacitance were measured by an AC impedance spectroscopy and DC electrical measurements as functions of relative humidity (RH) at 300 K.

2. Experimental

2.1. Materials

Pure alumina was prepared by calcination of a fibrous boehmite precursor prepared by a sol–gel process following a method mostly similar to that reported earlier by one of the present authors, Khalil [19]. In the method: the hydrolysis of aluminium *tri*-isopropoxide, $Al(OPr^i)_3$, dissolved in *n*-heptane was effected by a dropwise addition of a calculated amount of water to furnish the 1:1 water/alkoxy ratio. The solution was stirred magnetically at 400 rpm and this stirring was continued for 30 min, then the gel formed was allowed to age for 3 days. Subsequently, the gel was filtered off from its solution and allowed to dry at room temperature overnight followed by 24 h heating at 333 K in a drying furnace. Portion of the dried gel, has been characterized as boehmite, was calcined in a muffle furnace for 3 h at 873 K and stored for analyses.

NiO/alumina were prepared by mixing of alumina gels obtained by the hydrolysis of aluminium *tri*-isopropoxide, as above, after 1 h aging period; and the desired amount of Ni hydroxide gel, which was prepared as follows. A calculated amount of nickel nitrate hexahydrate, $Ni(NO_3)_2{\cdot}6H_2O$, corresponding to 5%, 10%, 20% or 30% w/w NiO/Al_2O_3 loading, was dissolved in a small portion of water. Hydrolysis was carried out by a dropwise addition of 10% solution of ammonium carbonate. A gel was formed after the later solution neutralizes the nitrate solution. The final pH value of the gel was adjusted to 9.5 by the addition of slight excess of the ammonium carbonate solution. For all the mixing ratios, the total volume of hydrolyzed nickel nitrate solutions (gels) was made the same.

Gel mixing was affected by the addition of the corresponding nickel hydroxide gel to the alumina gel and mixing was aided by magnetic stirring at 100 rpm for a 10-min period. The mixed gel was kept in a water bath at 323 K for 3 h and then aged for 3 days, dried, and calcined at 873 K for 3 h as done for the pure alumina. For simplicity, respective code numbers 600, 605, 610, 620, and 630 are designated for the test materials containing 0%, 5%, 10%, 20% and 30% w/w NiO/Al_2O_3.

2.2. Techniques

Nitrogen adsorption/desorption isotherms at 77 K were measured using a model ASAP 2010 (Micromeritics Instrument, USA). Prior to the measurements, all samples were outgassed for 2 h at 423 K to 0.1 Pa. The specific surface area, S_{BET}, was calculated by

applying the BET equation [20]. Assessment of microporosity was made from *t*-plot constructions, using the Harkins–Jura correlation [21] for *t*-plot as a function of normalized pressure, p/p_o. External surface area S_{Ext} (surface area due to nitrogen adsorption on mesopore and macropore surfaces, i.e. pores wider than 2 nm in diameter) were determined from slope analysis of the *t*-plots, following the *t*-plot method [22,23]. Micropore area, S_{mic} (surface area corresponding to the amount of nitrogen gas adsorbed in micropore <2 nm in diameter) for each sample was calculated by subtraction of S_{Ext} from the corresponding S_{BET} value, i.e. $S_{BET}=S_{mic}+S_{Ext}$. Average pore diameter was calculated from the ratio $4V_p/S_{BET}$ [24], where V_p is the specific pore volume.

X-ray diffraction (XRD) patterns were obtained using a Philips 1840 Diffraction system at room temperature using Cu-K_α radiation.

Magnetic susceptibility has been measured for the No. 620 and No. 630 materials using a magnetic susceptibility balance (Sherwood Scientific) that employs the conventional Gouy method.

Electrical measurements of the test materials are performed on pellets prepared by the same procedure and measured under the same geometry for all samples. A uniaxial force of 4 tons has been applied for a few minutes using a hydraulic press to form the resulting nanostructured powder into pellets of 1.0 mm thickness and 13 mm diameter. The pellets faces were coated with thin gold films using thermal evaporation to make good electrical contacts of 8.5 mm diameter. Samples were held between gold-coated electrodes with very slight spring pressure in a sample holder constructed from Teflon. This measuring cell was then inserted into the humidity chamber. Water saturated vapor was obtained by bubbling compressed air through deionized water at room temperature. Relative humidity (RH) was controlled between 1% and 92% by mixing absolutely dried air (RH = 0), rather dried air (RH = 18%) and water saturated air streams. Testo digital hygrometer was employed to monitor RH changes from 1% to 92%. The accuracy of the hygrometer was $\pm 2\%$ in the range of 5% to 95% with a resolution of 0.1%. All samples were subjected for drying at 473 K for 30 min prior to electrical measurements.

DC electrical measurements were performed using a Keithley 617 Electrometer at an applied voltage of 10 V. Impedance spectra were collected using an impedance gain-phase analyzer (Model SI 1260) in two-point configuration. Data were collected from 10 MHz to 0.1 Hz. The spectra obtained were analyzed for resistance and capacitance equivalent circuit elements vs. RH by a commercial software package.

3. Results and discussion

Structural information of the prepared materials can be realized by inspection of Fig. 1, which shows

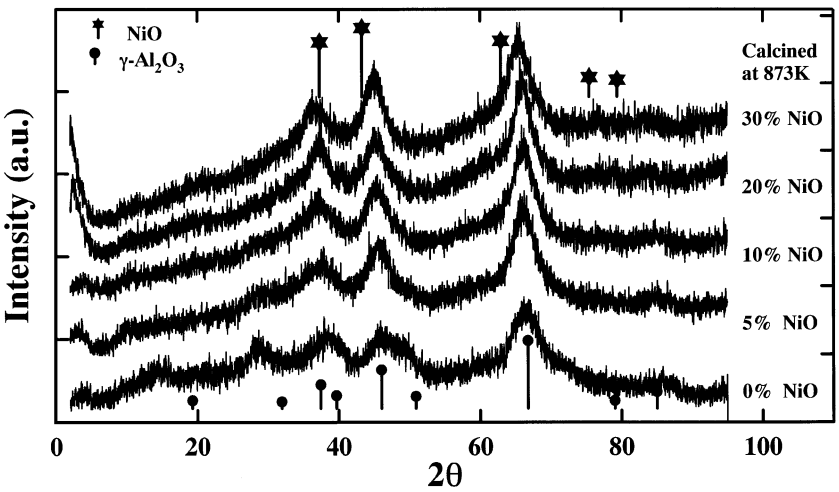

Fig. 1. XRD patterns of NiO/Al_2O_3 nanocomposite materials.

Table 1
Textural characteristics: S_{BET} surface area, micropore area S_{mic}, external surface area S_{Ext} along with the particle size for the test composite materials calcined at 873 K in air for 3 h

Sample CN	NiO/Al_2O_3 (w/w %)	S_{BET} (m^2/g)	S_{mic} (m^2/g)	S_{Ext} (m^2/g)	Average pore diameter (nm)
Pure Al_2O_3					
No. 600	0	288.6	40.0	248.6	15.8
No. 605	5	290.7	12.0	278.7	17.4
No. 610	10	341.0	6.2	334.7	12.5
No. 620	20	289.3	0.0	289.3	7.3
No. 630	30	267.0	0.0	267.0	5.4

$S_{BET} = S_{mic} + S_{Ext}$.

the XRD patterns measured for the test materials. According to the applied preparation method [19], short fibrous boehmite should be formed upon drying of the alumina gel and upon calcinations thermally stabilized transitional aluminas are formed, which preserve high surface area due to the fibrous nature of the precursor. Clearly, the pure alumina sample No. 600, which was calcined at 873 K for 3 h, shows a transitional alumina phase structure (γ-Al_2O_3) and preserves high surface area as expected, see Table 1. However, materials prepared by mixing of alumina gels with 5–30% w/w Ni hydroxide gel and subsequent drying and calcinations at 873 K for 3 h show similar XRD patterns of little improved crystallinity. This indicates that the addition of Ni hydroxide gel did not considerably interrupt the structural evolution of the transition alumina phase. Moreover, no sharp peaks were observed for NiO even for the No. 630 material which contains 30% w/w NiO/Al_2O_3 and calcined at 873 K for 3 h. This in fact suggested that NiO phase is actually present in the form of highly dispersed crystallites in the alumina matrix and/or in the form of $NiAl_2O_4$ phase. In fact, X-ray analysis is not informative in characterizing such systems due to the very close values of d-spacing of gamma alumina, and the spinel $NiAl_2O_4$ [25]. However, a slight peak shifts towards higher d-spacing was observed with the increase of NiO ratio. The increase of the d-spacing may be explained in terms of partial formation of NiO/γ-Al_2O_3 solid solution [25]. Textural characteristics including S_{BET} surface area, micropore area S_{mic}, external surface area S_{Ext} along with the average particle size for the test composite materials are displayed in Table 1. These data indicate that NiO loaded materials shows slightly higher surface area amount to ~ 290.7 m^2/g for the sample No. 605 in comparison to 288.6 m^2/g for the pure material (No. 600). Sample No. 610 shows even higher surface area amounts to 340 m^2/g. However, sample No. 620 shows a specific surface area that amounts to 289.3 m^2/g, which is lower than that of the No. 610 but still slightly higher than the pure one. These results indicate a uniform dispersion of NiO species through the surface of gamma alumina [26]. However, the decrease of specific surface area on going from the

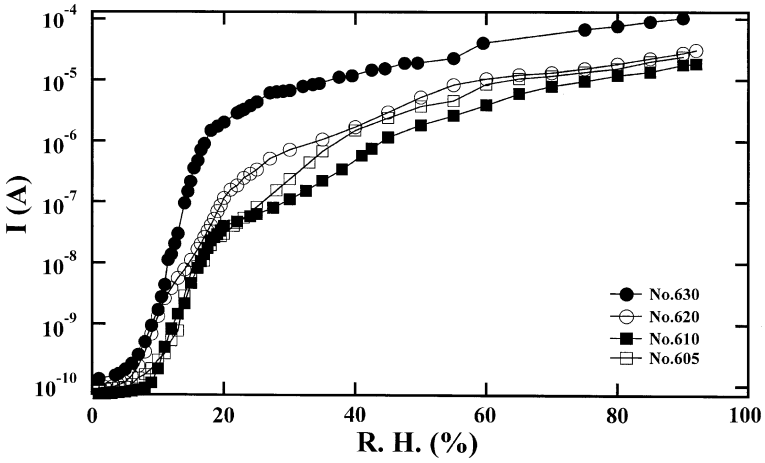

Fig. 2. DC current through NiO/Al_2O_3 nanocomposites measured as a function of RH.

sample No. 610 to sample No. 620, whereas NiO ratio is higher for the latter, may be explained in terms of the formation of relatively larger NiO particles after surface saturation with finally divided NiO species. Another important textural modification (Table 1) was revealed by the decrease of the average pore diameter (as 17.4, 12.5, 7.3, and 5.4 nm) upon the increase of NiO ratio (as 5%, 10%, 20%, and 30%), respectively.

The magnetic susceptibility of the No. 620 and No. 630 samples are measured using Gouy method. Large magnetic susceptibilities $\sim 5 \times 10^{-5}$ emu/g (NiO), comparable to those of various NiO catalysts [27], have been obtained indicating NiO nanoparticles in the γ-Al_2O_3 matrix. The large magnetic susceptibility of NiO nanoparticles compared with bulk antiferromagnetic (AF) NiO arises from incomplete magnetic compensation between AF coupled Ni ions on surface A and B magnetic sublattices of NiO AF nanoparticles [28]. It has been recently reported that the magnetic susceptibility of NiO measured at 300 K scales to its crystallite size as follows: $\chi_{NiO} = 9.0 \times 10^{-6} + (2.3 \times 10^{-4}/d)$, where d is the XRD particle size measured in nanometers [28]. The above expression has been used successfully for doped NiO, α-Al_2O_3 supported catalyst and coprecipitated NiO/γ-Al_2O_3 [27] in which a comparison between magnetic susceptibility per gram of NiO and XRD line broadening measurements were made. The drawback of this method is the presence of spinel $NiAl_2O_4$ that might occur when high concentrations of NiO on Al_2O_3 are heated at high temperatures, which is not considerably the case for our samples. However, the error introduced in the size determination is found to be insignificant for $NiAl_2O_4$ content below 5 wt.% [27]. The NiO particle size is estimated using the above equation to be 15 and 13 nm for samples No. 620 and No. 630, respectively.

Humidity sensing properties of the samples are shown in Fig. 2, which shows the current vs. RH at 300 K for all specimens. The points in the figure represent the experimental data and the lines are drawn to guide the eye. All currents are normalized to a sample thickness of 1 mm. The current, which is proportional to specimen conductivity, increases slightly as RH increases to about 5% and increases by about three orders of magnitude as the RH is increased from 5% to about 18% and extra three orders of magnitude when RH is increased from 20% to 92%. It should be noted that in general, for any RH values the current through the sample concerned increases for higher NiO content material. For example, the current through specimen No. 605 and No. 610 is almost the same particularly for RH less than 20%, increases through specimen No. 620 and that through specimen No. 630 is the highest. Humidity sensing characteristics have been studied

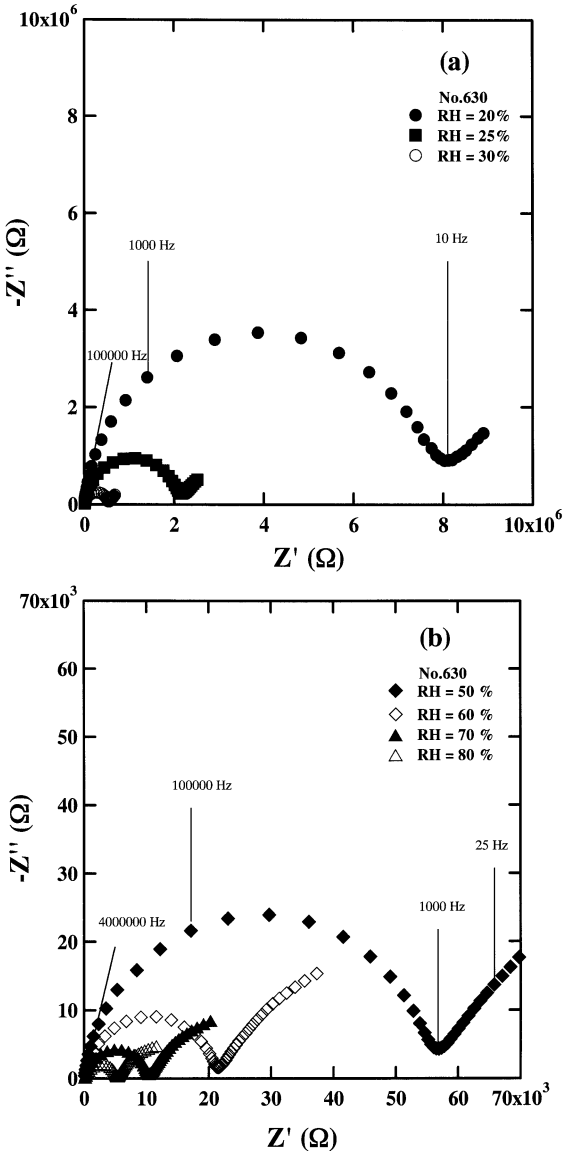

Fig. 3. The complex impedance spectra of NiO/Al_2O_3 nanocomposites measured as functions of RH.

earlier for a number of ceramic systems [29–32]. In the present series of samples, the conductance change was found to cover the range of 10^{-10} to 10^{-3} (Ω^{-1}). Therefore, it is evident that the test materials are sensitive towards RH and are comparable to other conventional ceramics, for which the conductance change was found to cover the range of 10^{-8} to 10^{-4} (Ω^{-1}).

Fig. 3a,b displays typical room temperature impedance spectra of a pressed powder of sample No. 630 at indicated RH. In each spectrum, the frequency decreases from left to right. Two arcs are obtained, an incomplete depressed arc at low frequency and a nearly perfect semicircular, centered on the real axis, at high frequency. The low frequency arc was ascribed to the electrode polarization arc on the basis of the capacitance obtained from equivalent circuit fitting (few μF), which was relatively insensitive to RH. The high frequency (bulk) arc shrinks significantly as RH is increased. Similar results are obtained for other samples with lower NiO content. For all spectra, the bulk arc was modeled as a resistor and capacitor in parallel. For all samples, the bulk impedance arcs are depressed below the real axis in Nyquist plots ($-Z''$ vs. Z'). Samples' capacitances and conductivities are calculated vs. specimen composition and RH. Capacitances for all samples for the whole RH range remain between 40 and 60 pF whereas conductivities depend on sample composition and strongly on RH. Resistances typically changes from $10^7$to 10^3, i.e. almost three to four orders of magnitude with increasing RH from 18% to 92% for all specimens.

The dependence of the bulk electric conductivity obtained from the IS measurements on NiO content is shown in Fig. 4 for various RH values. Accordingly, the conductivity slightly decreases with increasing NiO content from 5% to 10% and increases with further increase of NiO above 10%. The behavior can be understood in view of the morphological changes of the specimens when the NiO content is changed. The relative conductivity of the samples were in the order No. 605>No. 610<No. 620<No. 630. This order is exactly reversed for the S_{BET} values, which were in the order No. 605<No. 610>No. 620>No. 630. Therefore, the observed order of the materials conductivity may be explained as: when higher surface area is available for adsorption at a given humidity percentage (e.g. No. 610) the tendency for multilayer adsorption of water on the strong conduction centers might be decreased. This was because, as long as more exposed (free from adsorption) surface is present, water chemisorption rather than physisorption and multilayer formation is more likely to occur. This will decrease both the dissociation rate of physisorbed water and the production of protons responsible for the electrical conduction, simply because less physisorbed water is available. In addition, due to the increase of NiO ratio the textural data (Table 1) indicates the removal of microporosity and the shift of average pore diameter toward more reactive mesopore size (~ 5 nm for No. 630) facilitates better response for humidity.

There was however a noticeable hysteresis in resistance as RH is cycled from low RH to high

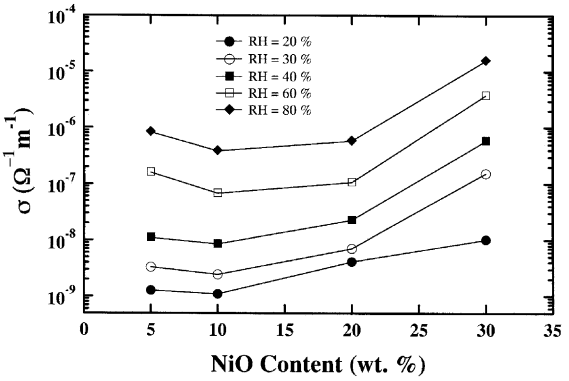

Fig. 4. Dependence of the electrical conductivity of NiO/Al_2O_3 nanocomposites on NiO content at indicated RH levels.

RH and back again. This is intimately due to different response and recovery time during increasing or decreasing RH, respectively. The time response of a sensor can vary from seconds to hours [33,34]. Thus, it is of interest to examine the test materials response and recovery time. Two samples have been examined in this regard. Sample No. 630, which has the highest electrical conductivity, has been examined using DC measurements for RH values less than 20%. The resistance in dry air (RH nominally 0%) as well as in an air stream of RH about 18% helped to establish the response and recovery characteristics for this sample at low RH levels. The sample was dried at 473 K for 30 min as was done before and then exposed to air stream of RH = 18%. Fig. 5a shows the DC current increasing by two orders of magnitude in a time interval $t_1 = 20$ min when RH is increased, whereas the time required to move between the same points when RH is decreased, t_1', is more than twice as large as t_1. For the second sample, No. 620, which is characterized with intermediate conduction, has been examined using IS for RH values larger than 20%. Again, the sample was dried at 473 K for 30 min and then exposed to an environment of RH = 18% for enough time to reach equilibrium. The sample is subsequently exposed to a vapor stream. Fig. 5b shows that the time required to increase its conductivity by two orders of magnitude is $t_2 = 30$ min whereas the time required to move between the same points when RH is decreased is $t_2' = 4t_2$. Ideally, a humidity sensor should follow the same conductance path when humidity is increased or decreased. However, as a matter of fact, most sensors exhibit some degree of hysteresis, whereby the conductance path differs to some extent. The present features, slow kinetics and irreversibility are the principle drawbacks to nanostructured humidity sensors [35]. This can be ascribed to the difficulty of evaporating water from the fine pore network as well as the thick pellets shape of our samples. Moreover, capillary forces, which are extremely strong at fine pore sizes, lead to perma-

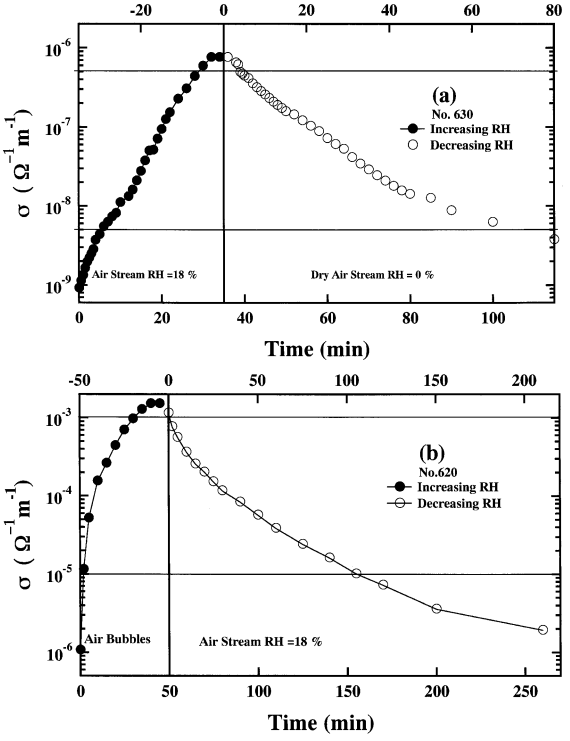

Fig. 5. Response and recovery characteristics of (a) No. 630 and (b) No. 620 NiO/Al_2O_3 nanocomposites.

nent changes in the microstructure with RH cycling, as evidenced by the hysteresis and time responses in the conductivity measurements. Indeed, all specimens retain their higher resistance $\sim 10^{10}$ Ω when dried at 473 K for 10 min.

Electrical conductivity σ and resistivity ρ are calculated as functions of RH from both DC and IS data. Fig. 6 displays σ and ρ of specimen No. 630 for the whole RH range. It is evident that σ changes exponentially as a function of RH with different slopes in low and high RH regions. It is noticed also that the DC conductivity is lower than that obtained from IS data for the same RH. It has been reported before [36] that the presence of hydroxyl ions on the oxide surface promotes the dissociate hydroxyl and provides protons as charge carriers. These protons hop between adjacent hydroxyl groups giving rise to electrical conductivity. The change of the electrical conductivity has been shown by various investigators to be almost exponential with RH [36,37]. From Fig. 6, it is clear that the change of σ is exponential as a function of RH—with different slopes in low and high RH regions owing to different activation energies for proton transport. As has been stated above, the current (hence electrical conductivity) at certain RH increases with increasing NiO content in our specimens. Conductivity of NiO nanoparticles has been ascribed to Ni^{2+} vacancies [37–39]. Each Ni^{2+} vacancy in the lattice transforms two adjacent Ni^{2+} ions into Ni^{3+} ions in accordance with charge neutrality. As far as the particle size do not increase with increasing NiO content in our composites, as evidenced by the particle size obtained from magnetic susceptibility data, increasing the NiO content should be accompanied by higher Ni^{2+}vacancy density and higher density of Ni^{3+} ions. These Ni^{3+} ions are believed to provide the sites for chemisorption of the hydroxyl groups. Upon exposing a dry ceramic oxide to humid environment, a layer of water vapor molecules is first chemisorbed with the formation of surface hydroxyl ions on its surface. Charge transport occurs firstly by a hopping mechanism between hydroxyl groups of protons coming from the hydroxyl dissociation. With increasing humidity levels, water molecules are physically adsorbed on the top of the chemisorbed hydroxyl layers, which increase the number of protons available for electrical conduction. This explains the increase in electrical conductivity through specimens with larger NiO content at a constant RH. It should be mentioned that partial formation of $NiAl_2O_4$ phase, which may occur, has not been considered in the above discussion.

The capacitances obtained from fitting of high frequency arc have been used to calculate the effective dielectric constant, assuming infinite parallel plate geometry, of NiO/Al_2O_3 nanocomposites in humid environments. The effective dielectric constant was found to be close to 80. Realistic values for our samples should be about 20% lower, which would better fit to the expected values between alumina and water. The lines in Fig. 7 represent the predicted behavior if the effective capacitance is governed by the solid phases ($\varepsilon = 10$ for NiO and Al_2O_3) or by the water phase ($\varepsilon = 80$ for H_2O). The behavior is consistent with a continuous water phase at RH ≥ 18% for all

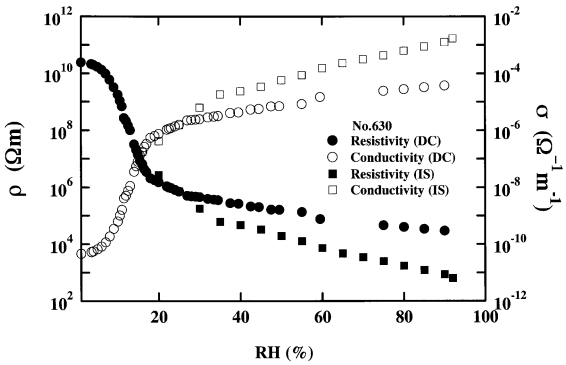

Fig. 6. Electrical conductivity and resistivity of No. 630 nanocomposite calculated from DC and IS measurements as functions of RH.

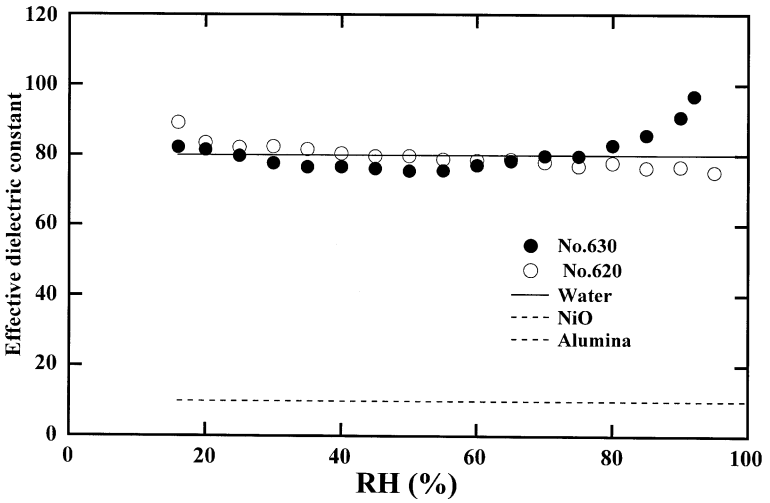

Fig. 7. Effective dielectric constant of NiO/Al_2O_3 nanocomposites as a function of RH.

compositions. Humidity sensing characteristics in the case of ceramic systems have been ascribed to absorption of water molecules on their surface [32,36]. It can be concluded that in the present system the electrical conductivity changes as a function of RH arise due to an ionic transport.

4. Conclusion

Electrical conductance for sol–gel derived high surface area NiO/Al_2O_3 nanocomposite materials was found to be very sensitive to air humidity. Electrical conductance increases as a function of RH by about six orders of magnitude in the range of 5–90%. The increase of NiO content was found to increase the electrical conductances in humid air. From the texture point of view and within the investigated group of materials, the removal of microporosity as well as the decrease of the average pore diameters due to the increase of NiO ratio allows better response for humidity. The capacitances obtained suggest that the electrical properties of NiO/Al_2O_3 nanocomposites in moist environments are dominated by the condensed water phase in the pore network. The humidity sensing behavior of NiO/Al_2O_3 nanocomposite is controlled by the ionic conduction through the adsorbed water phase.

Acknowledgements

This work was supported by Grant No. 00/11-2-04 given by Research Council, UAEU.

References

[1] H. Gleiter, Prog. Mater. Sci. 33 (1989) 223.
[2] R.W. Siegel, MRS Bull. 15 (1990) 60.
[3] R.W. Siegel, Annu. Rev. Mater. Sci. 21 (1991) 559.
[4] R.W. Siegel, Processing of metals and alloys, in: R.W. Chan (Ed.), Materials Science and Technology, vol. 15, VCH, Wienheim, Germany, 1991, pp. 583–614.
[5] H. Gleiter, Nanostruct. Mater. 1 (1992) 1.
[6] R.W. Siegel, in: F.E. Fujita (Ed.), Physics of New Materials, Springer-Verlag, Berlin, 1994, pp. 65–105.
[7] C.J. Brinker, G.W. Scherer, Sol–Gel Science, Academic Press, Boston, 1990.
[8] K.M.S. Khalil, A.A. Elsamahy, M.S. Elanany, J. Colloid Interface Sci. 249 (2002) 359.
[9] G. Gusmano, G. Montesperelli, B. Morten, M. Prudenziati, A. Pumo, E. Traversa, J. Mater. Process. Technol. 56 (1996) 589; K.I. Arshak, K. Twomey, Microelectron. J. 33 (2002) 213.
[10] Y. Shimizu, R. Arai, T. Seiyama, Sens. Actuators 7 (1985) 11.
[11] G. Gusmano, G. Montesperelli, E. Traversa, G. Mattogno, J. Am. Ceram. Soc. 76 (1993) 743.
[12] J.H. Anderson, G.A. Parks, J. Phys. Chem. 72 (1968) 3662.
[13] G. Gusmano, G. Montesperelli, P. Nunziante, E. Traversa, Br. Ceram. Trans. 92 (1993) 3.
[14] M.J. Madou, S.R. Morrison, Chemical Sensing with Solid State Devices, Academic Press, San Diego, CA, 1989, p. 506.

[15] C.-W. Lee, H.-W. Rhee, M.-S. Gong, Synth. Met. 106 (1999) 177;
M. Campos, G.C. Miceli, N. Gamaioni, G. Chiodelli, Synth. Met. 73 (1995) 131.
[16] P. Chauhan, S. Annapoormi, S.K. Trikha, Thin Solid Films 346 (1999) 226.
[17] Y. Ushio, M. Miyayama, H. Yanagida, Sens. Actuators, B 17 (1994) 221.
[18] J.R. Macdonald (Ed.), Impedance Spectroscopy, Wiley, New York, 1987, pp. 13, 14, 205.
[19] K.M.S. Khalil, J. Catal. 178 (1998) 198.
[20] B. Brunauer, P.H. Emmett, E. Teller, J. Am. Chem. Soc. 60 (1938) 309.
[21] W.D. Harkins, G. Jura, J. Chem. Phys. 11 (1943) 431.
[22] F. Rouquerol, J. Rouquerol, K. Sing, Adsorption by Powders and Porous Solids, Academic Press, London, 1999.
[23] B.E. Handy, M. Maciejewski, A. Baiker, A. Wokaun, J. Mater. Chem. 2 (1992) 833.
[24] D.H. Everett, in: D.H. Everett, F.S. Stone (Eds.), Structure and Properties of Porous Materials, Butterworths, London, 1958, p. 95.
[25] E. Kis, R.M. Neducin, G. Lomic, G. Boskovic, D.Z. Obadovic, J. Kiurski, P. Putanov, Polyhedron 17 (1998) 27.
[26] T. Osaki, T. Hiriuchi, T. Sugiyama, K. Suzuki, T. Mori, J. Non-Cryst. Solids 225 (1998) 111.
[27] J.T. Richardson, M.V. Twigg, J. Catal. 188 (1999) 226 (and references therein).
[28] J.T. Richardson, D.I. Yiagas, B. Turk, K. Foster, M.V. Twigg, J. Appl. Phys. 70 (1991) 6977.
[29] G. Gusmano, G. Montesperelli, P. Nunziante, E. Traversa, Br. Ceram. Trans. 92 (1993) 104.
[30] T. Nitta, in: T. Seiyama (Ed.), Chemical Sensor Technology, vol. 1, Elsevier, Amsterdam, 1988, p. 57.
[31] Y. Yokomizo, S. Uno, M. Harata, H. Hiraki, K. Yuki, Sens. Actuators 4 (1983) 599.
[32] D. Das, M. Pal, E. Di Bartolomeo, E. Traversa, D. Chakravorty, J. Appl. Phys. 88 (2000) 6856.
[33] Thermoset polymer-based capacitive sensors, applications sheet, www.honeywell.com/sensing and humidity probes data sheet, www.vernier.com.
[34] Gas detection systems, data sheet, www.scottinstruments.com.
[35] J.-H. Hwang, T.O. Mason, M.F. Buehler, J.G. Darab, D.W. Matson, J.C. Linehan, Mater. Sci. Eng., A 204 (1995) 225.
[36] J. Anderson, G.A. Parkes, J. Phys. Chem. 72 (1968) 3662.
[37] F.J. Morin, Phys. Rev., B 93 (6) (1954) 1199.
[38] D. Adler, J. Feinleib, Phys. Rev., B 2 (8) (1970) 3112.
[39] V. Biju, M. Abdul Khadar, Res. Bull. 36 (2001) 21.